Clays and Clay Minerals, Vol. 55, No. 1, 96–107, 2007.

NONTRONITE PARTICLE AGGREGATION INDUCED BY MICROBIAL Fe(III) REDUCTION AND EXOPOLYSACCHARIDE PRODUCTION

DEB P. JAISI[1], HAILIANG DONG[1,*], JINWOOK KIM[2], ZIQI HE[3] AND JOHN P. MORTON[1]

[1] Department of Geology, Miami University, Oxford, OH 45056, USA
[2] Naval Research Laboratory, NASA Stennis Space Center, MS 39529, USA
[3] Department of Civil & Environmental Engineering and Geodetic Science, The Ohio State University, Columbus, OH 43210, USA

Abstract—Clay particle aggregation affects a number of environmental processes, such as contaminant sorption/desorption, particle movement/deposition, and sediment structure and stability, yet factors that control clay aggregation are not well understood. This study was designed to investigate how microbial reduction of Fe(III) in clay structure, a common process in soils and sediments, affects clay-particle aggregation. Microbial Fe(III) reduction experiments were conducted with *Shewanella putrefaciens* CN32 in bicarbonate buffer with structural Fe (III) in nontronite as the sole electron acceptor, lactate as the sole electron donor, and AQDS as an electron shuttle. Four size fractions of nontronite (D_5-D_{95} of 0.12–0.22 μm, 0.41–0.69 μm, 0.73–0.96 μm and 1.42–1.78 μm) were used to evaluate size-dependent aggregation kinetics. The extent of Fe(III) bioreduction and the amount of exopolysaccharide (EPS), a major biopolymer secreted by CN32 cells during Fe(III) bioreduction, were measured with chemical methods. Nontronite particle aggregation was determined by photon correlation spectroscopy and scanning electron microscopy. The maximum extent of Fe(III) bioreduction reached 36% and 24% for the smallest and the largest size fractions, respectively. Within the same time duration, the effective diameter, measured at 95% percentile (D_{95}), increased by a factor of 43.7 and 7.7 for these two fractions, respectively. Because there was production of EPS by CN32 cells during Fe(III) reduction, it was difficult to assess the relative role of Fe(III) bioreduction and EPS bridging in particle aggregation. Thus, additional experiments were performed. Reduction of Fe(III) by dithionite was designed to examine the effect of Fe(III) reduction, and pure EPS isolated from CN32 cells was used to examine the effect of EPS. The data showed that both Fe(III) reduction and EPS were important in promoting clay mineral aggregation. In natural environments, the relative importance of these two factors may be dependent on local conditions. These results have important implications for understanding factors in controlling clay particle aggregation in natural environments.

Key Words—Aggregation, Electrophoretic Mobility, EPS, Fe(III) Reduction, Nontronite, SEM, *Shewanella Putrefaciens*.

INTRODUCTION

Aggregation of suspended particles exerts an important influence on contaminant sorption/desorption (Pignatello *et al.*, 1996; Dachs and Bayona, 1997), particle movement/deposition (O'Melia *et al.*, 1980), vertical transfer of particles (Hill, 1996), and sediment structure and stability (Theilen and Pecher, 1991). Previously, particle concentration, solution chemistry (ionic strength), type and conformational nature of the surface polymers (in polymer bridging), and surface charge/Fe(III) reduction were considered as major factors that control particle aggregation (Olness and Clapp, 1975; Theng, 1979; Chenu *et al.*, 1979; Kim *et al.*, 2005). Among these factors, the importance of polymer bridging in promoting particle aggregation has long been recognized (Healy and la Mer, 1964; Hoggs, 1984; Moudgil *et al.*, 1987; Elimelich *et al.*, 1995). The long-chain polymers may attach to particles and bridge them to form aggregates, even though the particles are electrostatically repulsive (Elimelich *et al.*, 1995). Natural and synthetic polymers have been used extensively to understand their roles in inter-particle bridging and resulting flocculation in ore-processing industries (Fuller *et al.*, 1995; Yuehena *et al.*, 2004), wastewater treatments (Bura *et al.*, 1998; Liao *et al.*, 2001; Walker and Bob, 2001; Droppo and Irvine, 2002), marine sediments dynamics (Tolhurst *et al.* 2002; Orton and Kineke, 2001; Hill *et al.* 2001), and soil amendments (de Boodt, 1990). These studies focused primarily on sorption and conformation of externally added model polymers to achieve desired properties (such as aggregation, dispersion) without any structural changes in sorbent properties.

Clays and clay minerals are major components in soils, sedimentary rocks and pelagic oozes blanketing the ocean basins (Moore and Reynolds, 1997). They play an important role in environmental processes such as nutrient cycling, plant growth, contaminant migration, organic matter maturation, and petroleum production (Stucki *et al.*, 2002; Kim *et al.*, 2004; Stucki, 2006). The changes in the oxidation state of the structural Fe in clay minerals, in part, control the mobility and stability of

* E-mail address of corresponding author:
dongh@muohio.edu
DOI: 10.1346/CCMN.2007.0550108

Copyright © 2007, The Clay Minerals Society

https://doi.org/10.1346/CCMN.2007.0550108 Published online by Cambridge University Press

clay minerals in natural environments (Stucki *et al.*, 2002). The structural ferric iron [Fe(III)] can be reduced either chemically or biologically (Gates *et al.*, 1993; 1998; Kostka *et al.*, 1996, 1999a, 1999b; Dong *et al.*, 2003; Kim *et al.*, 2004; Jaisi *et al.*, 2005; Stucki, 2006). Recently, it has been found that biological Fe(III) reduction can promote clay particle flocculation (Gates *et al.*, 1998; Kim *et al.*, 2005). However, little attention has been given to the effects of biopolymers secreted by cells during Fe(III) bioreduction on clay particle aggregation. The relative importance of Fe(III) reduction and biopolymer production in clay particle aggregation has not yet been investigated.

The objective of this research was, therefore, to determine how Fe(III) bioreduction and biopolymer production promote clay particle aggregation. We quantified the extent of Fe(III) bioreduction and production of exopolysaccharide (EPS) by *Shewanella putrefaciens* CN32 cells during reduction of Fe(III) in nontronite. We measured changes in aggregation rate for the various sizes of nontronite particles over the course of Fe(III) bioreduction to investigate size-dependent aggregation kinetics. In this paper, we used a generic term 'aggregation' broadly to include all processes that lead to increase in particle dimension without identifying underlying mechanisms (such as coagulation, flocculation, agglutination, *etc*.). The results of this study have important implications for understanding clay-particle aggregation kinetics as a result of Fe(III) reduction and biopolymer bridging.

MATERIALS AND METHODS

Mineral and bacteria preparation

Nontronite from Uley graphite mine, South Australia (The Clay Minerals Society Reference Clay NAu-2) (Keeling *et al.*, 2000) was chosen in this study, because it had a large Fe(III) content and a significant amount of it could be reduced by bacteria (Jaisi *et al.*, 2005). Thus, the effect of Fe(III) reduction on particle aggregation could be readily observed. The NAu-2 sample was pure without any other Fe-bearing minerals and it contained 23.4% total Fe in its structure with almost all (99.8%) Fe as Fe(III) (Keeling *et al.*, 2000; Jaisi *et al.*, 2005).

Nontronite samples were first thoroughly soaked and then briefly sonificated in an ultrasonic water bath. To minimize any external stress, the soaked sample was stirred slightly and the resulting suspension was centrifuged to obtain different size fractions. Four size fractions (D_5-D_{95} of 0.12−0.22, 0.41−0.69, 0.73−0.96 and 1.42−1.78 μm; where D_x was the particle size at x percentile) were used for aggregation experiments. The size distribution in each fraction was measured by photon correlation spectroscopy (PCS) and scanning electron microscopy (SEM) image analysis. The BET surface area of these size fractions was measured using a Coulter SA3100.

Shewanella putrefaciens CN32 was originally isolated from a subsurface core sample (250 m beneath the surface) obtained from the Morrison Formation, a formation mined extensively for U, during drilling of a shale-sandstone sequence in northwestern New Mexico (Fredrickson *et al.*, 1998). CN32 was routinely cultured aerobically in tryptic soy broth (30 g/L) from the stock culture, which was kept in 40% glycerol at -80ºC. After harvesting in TSB until mid- to late-log phase, CN32 cells were washed three times in bicarbonate buffer. The initial cell density of all cultures was measured by both acridine orange direct count (AODC) and viable cell count.

Bacterial Fe(III) reduction experiments

Fe(III) bioreduction experiments were performed in bicarbonate buffer (25 mM) with Fe(III) in nontronite as the sole electron acceptor, lactate (10 mM) as the sole electron donor, and CN32 cells as a mediator in the presence of AQDS (0.1 mM) as an electron shuttle. The concentration of nontronite was fixed at 1 mg/mL, and cell density at ~2.1×10^7/mL. The experiments were performed with and without Na pyrophosphate as a dispersant (25 mM) with shaking in a water bath at 60 rpm and 25ºC. A concentration of Na pyrophosphate at 25 mM was found to be optimal to disperse individual clay particles without interfering with microbial bioreduction. Typically, duplicate experiments were prepared for each treatment. The extent of Fe(III) reduction was measured by Ferrozine assay (Stookey, 1970). The details of the experimental set up and measurements have been described previously (Jaisi *et al.*, 2005). The bioreduction experiments were typically run for 2 weeks. Some select bioreduction experiments were run shorter (in the range of 56 to 90 h) without shaking for the purpose of comparing two methods of particle-size measurements, *i.e.* PCS and SEM. The control tubes consisted of sterile bicarbonate buffer in place of CN32 cells.

Measurement of exopolysaccharide (EPS)

To study the effects of EPS on particle aggregation, EPS was extracted at selected times during Fe(III) bioreduction using the method by Tallon *et al.* (2003). Briefly, 3 mL of bacteria-clay suspension were centrifuged at 15,000 *g* for 15 min at 4ºC. The resulting pellet was washed with 3 mL of sterile 1 M NaCl solution followed by centrifugation at 15,000 *g* for 15 min at 4ºC. The viscous pellet was resuspended in 3 mL of 50 mM EDTA. The mixture was incubated for 4 h at 4ºC with frequent gentle agitation and then centrifuged at 6000 *g* for 30 min at 4ºC. The EPS was precipitated from the supernatant liquid by addition of two volumes of cold ethanol followed by an overnight incubation at 4ºC. The carbohydrate and protein fractions, the two major components of EPS, were quantified. The carbohydrate fraction was quantified according to the

https://doi.org/10.1346/CCMN.2007.0550108 Published online by Cambridge University Press

standard phenol/sulfuric acid method (Dubois *et al.*, 1956) and the protein fraction by the Bradford assay (Bradford, 1976). Glucose and protein (BSA, Sigma-Aldrich, St. Louis, Missouri) were used as standards in the quantification procedure. The protein and carbohydrate standards were prepared in the same matrix (nontronite at 1 mg/mL).

Particle-size measurement by photon correlation spectroscopy

Nontronite particle aggregation during Fe(III) bioreduction was determined by PCS using a 90Plus Particle Size Analyzer (Brookhaven Instruments Corporation, New York). The random intensity fluctuations in scattered laser light arising from the Brownian motion of nontronite particles were analyzed to give complete size distribution. One sample tube was sacrificed for each measurement from a set of identically treated experimental tubes.

Particle-size measurement by SEM image analysis

The PCS measurement was limited to particles <~2 μm in dilute clay suspension. Because particle size and concentration in some of our experiments exceeded the PCS limits, SEM image analysis was utilized instead. Initially, several trial experiments were performed to identify the optimum particle concentration. To prepare samples for SEM observation, a droplet of cell-clay mineral suspension was spread onto an ethanol-cleaned glass cover slip that was pre-treated with poly-E-lysine as an adhesive. Scanning electron microscopy images of air-dried nontronite particles were collected using a Zeiss Supra 35 VP SEM operated at an accelerating voltage of 10−15 kV and a working distance of 8−15 mm. Multiple images were taken from each sample over the course of the bioreduction experiment. At least 1500 particles were analyzed for each time point using the Image J software (NIH) to determine particle-size distribution. The particle outline was traced and the surface area of each outlined particle was calculated. Image artifacts (if any) resulting from particle overlapping or uneven brightness/contrast were excluded manually. The accuracy of the method was periodically checked using images of known surface area that were stored internally within the software. The particle size of the stored images could be calculated with the surface area approach described above and measured manually. The results obtained were consistent with the expected values, showing that the Image J software successfully measured the surface area of nontronite particles. The measured surface area of each particle was then converted to the effective diameter of a sphere. Although the shape of the original nontronite particles in unreduced samples was not spherical, aggregates appeared to be largely spherical or equidimensional. Nevertheless, it was only an approximation.

Measurement of electrophoretic mobility

Because bulk surface charge affects the rate of clay particle aggregation (Theng, 1979), electrophoretic mobility (EPM) was thus measured over the course of the Fe(III) bioreduction using Doppler electrophoretic light scattering analysis (DELSA) (Coulter DELSA 440 SX, Coulter Corporation, Miami, Florida). It utilizes a laser light, four photodiodes and four 256-channel autocorrelators to discriminate between particles from four optimized angles. This instrument is capable of discriminating electrophoretic heterogeneity and diffusion heterogeneity. All results were expressed in EPM, without converting it to zeta potential. This conversion, which employs the Smoluchowski approximation (double layer thickness is small compared to colloidal diameter; Hunter, 1981), may not be valid for growing clay particles. The experimental details of measurements are described elsewhere (Xu, 1993; Dong, 2002).

Bioreduced nontronite samples for the EPM measurement were prepared inside an anaerobic glove box (Coy Laboratory Products, Grass Lake, Michigan). After the sample cell was filled with clay suspension, it was sealed with Seal View® to prevent reoxidation of nontronite suspension during measurement. For coarse particles, which may undergo settling during measurement, EPM was measured at both the upper and lower stationary layers. Each reported mobility value represented an average of at least four measurements. The experimental conditions were as follows: temperature: 25ºC, frequency range: 500 Hz, electric field strength: 6 V, on-time: 2.5 s, and off-time 0.5 s. Typical temperature drifts within a single experiment were <0.1ºC so the effects of convection arising from Joule heating were minimized. The conductivity of nontronite suspensions was also measured to determine any changes in ionic strength of cell-clay suspension as a result of bioreduction.

Nontronite particle aggregation as a result of chemical reduction

To separate the effects of Fe(III) reduction and EPS bridging on nontronite particle aggregation, separate experiments were performed using nontronite reduced chemically by Na dithionite (Stucki *et al.*, 1984). The objective here was to reduce Fe(III) in nontronite to varying extents (*i.e.* 18%, 38%, 49%, 64% and 98%) so that particle aggregation could be correlated with the extent of Fe(III) reduction. To achieve a specific extent of Fe(III) reduction, a stoichiometric amount of Na dithionite was added to each sample tube containing 5 mg/mL clay suspension. After 24 h of reduction, the extent of Fe(III) reduction was measured by the Ferrozine method (Stookey, 1970). Our separate experiments showed that Fe(III) reduction in nontronite by Na dithionite reached completion within a few hours. The reduced nontronite was separated from the dithionite solution by centrifugation and then washed four times with anaerobic bicarbonate buffer.

https://doi.org/10.1346/CCMN.2007.0550108 Published online by Cambridge University Press

Concentrations of cations released during partial dissolution of nontronite (such as Si, Al, K, *etc*.) as a result of Fe(III) reduction by dithionite were measured to understand the effects of released cations on particle aggregation. After washing the chemically reduced nontronite four times with anaerobic bicarbonate buffer, those cations that still remained sorbed onto nontronite particle surfaces were released into aqueous solution by decreasing the pH value to the point of zero net charge for nontronite (pH_{PNZC} = 2.1). The cation concentrations were measured by direct current plasma (DCP) emission spectroscopy (Katoh *et al.*, 1999). The chemically reduced nontronite (up to 98% of Fe(III) reduction) was then dispersed in bicarbonate buffer (at a final clay concentration of 1 mg/mL) and the time-course aggregation was performed with gentle shaking in a water bath at 60 RPM and 25ºC. The change in particle size with time was measured using the SEM method.

Nontronite particle aggregation as a result of EPS bridging

To identify the role of EPS bridging in nontronite particle aggregation, separate experiments were performed with purified EPS. The EPS produced by CN32 cells during Fe(III) bioreduction was extracted using the Tallon *et al.* (2003) method. Two separate aggregation experiments were performed with the 0.73−0.96 μm fraction (the same size fraction as that used for testing the effect of Fe(III) reduction) at two different concentrations of EPS, *i.e*. 50 mg/L and 800 mg/L. These two concentrations were representative of EPS production during Fe(III) bioreduction and corresponded to ~18% and 36% Fe(III) bioreduction, respectively. Particle aggregation with time was measured using the SEM method.

Transmission electron microscopy

To observe cell-particle associations at high resolution, both unreduced (control) and bioreduced samples were imbedded with Nanoplast resin and sliced using a microtome for transmission electron microscopy (TEM) observations (Kim *et al.*, 2004, 2005). The hydrophilic Nanoplast resin was preferred over classical L.R. White resin because the former does not require a solvent exchange (methanol/water exchange) step, which can cause artifacts, such as dissolution of organic matter. A JEOL 3010 TEM operating at 300 keV with a LaB_6 filament was used for all TEM analyses.

RESULTS

Methods of measuring particle aggregation − comparison between PCS and SEM

For the purpose of measuring nontronite particle size with these two methods, bioreduction experiments of shorter duration were run (for 60 h only). The extent of Fe(III) reduced during the first 60 h varied from 11.8% for the coarsest size fraction (1.42−1.78 μm) to 12.8% for the finest size fraction (0.12−0.22 μm). The particle-size distribution as measured by PCS for the 1.42−1.78 μm size fraction showed an increase in uniformity coefficient (Cu) [where $Cu = D_{60}/D_{10}$] with increasing incubation time (Figure 1a). A limited number of large particles aggregated fast, whereas the majority of particles remained at the same size or only slightly aggregated. For this reason and for clarity of data presentation, particle aggregation was expressed as an increase in the D_{95} percentile with time. D_{95} denoted a particular size in the distribution that 95% (by mass) of all measured particles had sizes either equal to, or smaller than, this value. The D_{95} value in all size fractions (Figure 1b) showed an initially high rate of aggregation (for the first 4 h) followed by a steady rate. The aggregation rate was greater for the finer size fractions. For example, during the first 60 h, the D_{95} value increased by a factor of 3.2 and 1.9 for the finest (0.12−0.22 μm) and the coarsest (1.42−1.78 μm) fractions, respectively (Figure 1b). The controls without CN32 cells did not show any measurable particle aggregation (data not shown).

During the same period (60 h), the SEM-measured D_{95} value of nontronite particles increased by a factor of 2.5 and 1.8 for the same two size fractions 0.12−0.22 and 1.42−1.78 μm, respectively (Figure 1b). Although the magnitude of increase in size was similar with the two methods, the SEM-measured particle size was smaller by 11−20%. This discrepancy may be caused by the different sample preparation procedure. Whereas clay suspension was directly used for the PCS measurement, SEM observations required drying of the clay suspension. Nontronite particles were expected to collapse upon drying. Nonetheless, the comparable magnitude of increase in particle size as measured by these two methods suggested that SEM image analysis was adequate to measure particle aggregation. Unlike the PCS method, the SEM image analysis method was not limited to a certain particle-size range and clay concentration. The method also had a high throughput.

Bacterial Fe(III) reduction

The extent of Fe(III) bioreduction increased with decreasing particle size (Figure 2a). The observed maximum extent of reduction in the finest and coarsest size fraction (0.12−0.22 μm and 1.42−1.78 μm) was 36.2% and 23.4%, respectively, suggesting a surface area effect. However, the extent of reduction normalized to surface area (Figure 2b) was greatest for the coarsest size fraction. The three finer fractions had similar extents of reduction when they were normalized in the same way. The rate of Fe(III) bioreduction was also size-dependent. The finer size fractions showed a greater rate of reduction and required more time to reach the maximum extent of bioreduction than the coarser ones. The controls did not show any measurable amount of Fe(III) reduction.

https://doi.org/10.1346/CCMN.2007.0550108 Published online by Cambridge University Press

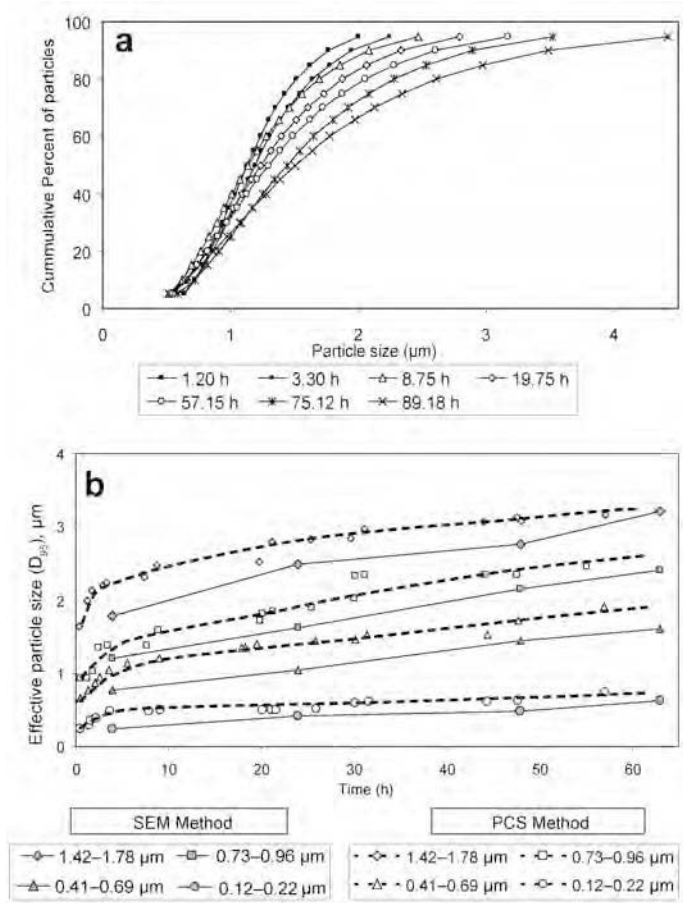

Figure 1. (a) Change in the distribution of particle size of the 1.42–1.78 μm fraction over the course of bioreduction (90 h). The size distribution was measured by the PCS method. (b) Change in particle size at 95% percentile (D_{95}) with time for four size fractions used in this study. The dotted lines represent the data obtained by the PCS method and the solid lines are those by the SEM method. The experiments were performed with 25 mM of Na pyrophosphate without shaking. The dotted lines are shown to elucidate the data trend, and are not model fits.

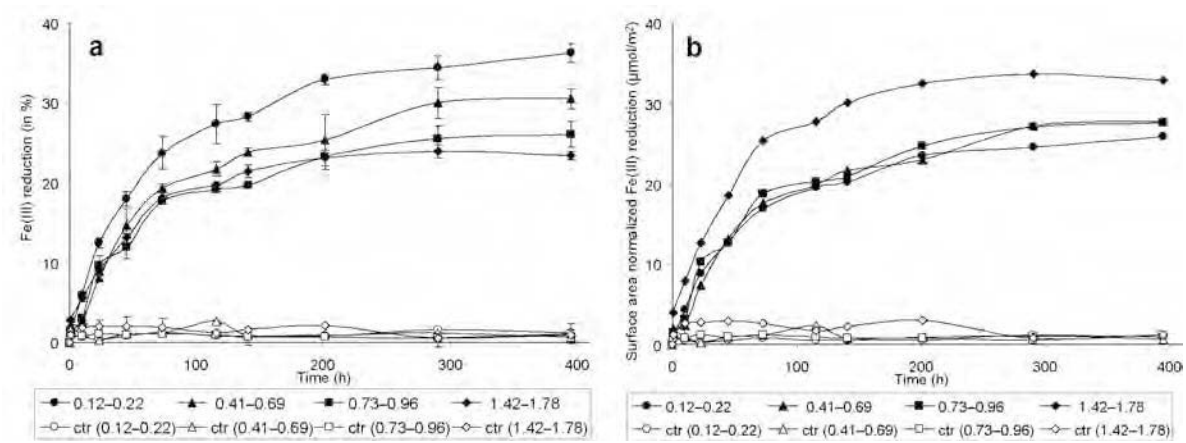

Figure 2. (a) Time-course Fe(III) reduction (expressed in percent) for the four size fractions of nontronite as measured by 0.5 N HCl extraction. Experiments were performed with shaking but no Na pyrophosphate. (b) Surface-area normalized Fe(III) reduction. The BET surface area of the size fractions of 0.12–0.22, 0.41–0.69, 0.73–0.96 and 1.42–1.78 μm was 29, 39, 45 and 52 m^2/g, respectively. The ctr symbols denote data for abiotic controls (no cells added).

https://doi.org/10.1346/CCMN.2007.0550108 Published online by Cambridge University Press

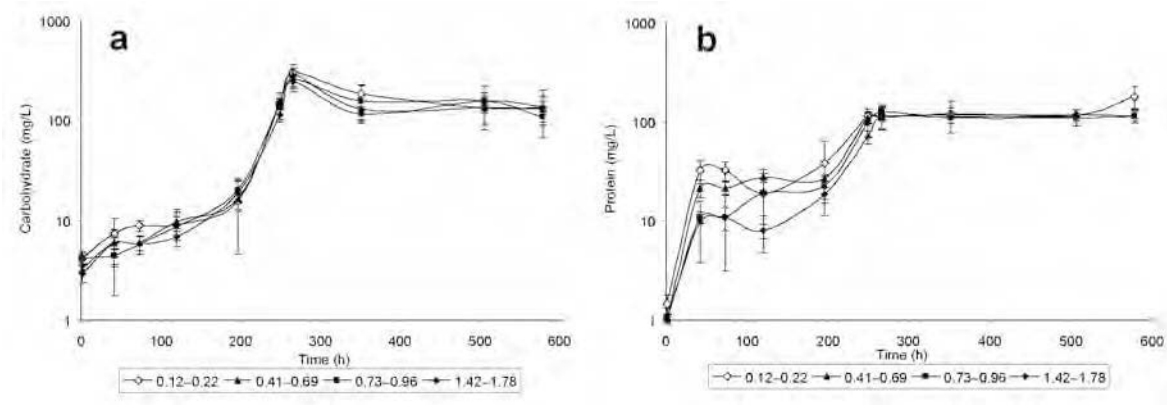

Figure 3. Time-course production of the carbohydrate (a) and protein (b) fraction of exopolysaccharide produced by CN32 cells during Fe(III) bioreduction.

Production of EPS during bioreduction and its role in particle aggregation

The carbohydrate and protein fraction, two major components of EPS, was determined to be 24% (by wt.) and 31% (by wt.) of the total amount of EPS, respectively. These two fractions increased steadily with time of bioreduction (Figure 3). Rapid EPS production occurred in the first 266 h and this period corresponded to the high rate of Fe(III) reduction. After 266 h, EPS production largely ceased, which again corresponded to a slow rate of Fe(III) bioreduction (Figure 2).

Electrophoretic mobility

The measured conductivity of the bacteria-nontronite suspension remained constant during the reduction experiment (0.91±0.04 mS), suggesting that few cations were released into aqueous solution as free ions. The electrophoretic mobility (EPM) values of nontronite suspensions changed over the course of Fe(III) bioreduction. At the early stage, the EPM values for the finer size fractions (0.12−0.22 and 0.41−0.69 μm) were more negative than those for the coarser ones (-3.5×10^{-8} *vs.* -3×10^{-8} $m^2/V-s$), but later the relative magnitude reversed (Figure 4). For the coarser two fractions, the measured EPM remained nearly constant at -3.15×10^{-8} ($\pm 0.2 \times 10^{-8}$) $m^2/V-s$ for the entire duration of Fe(III) bioreduction.

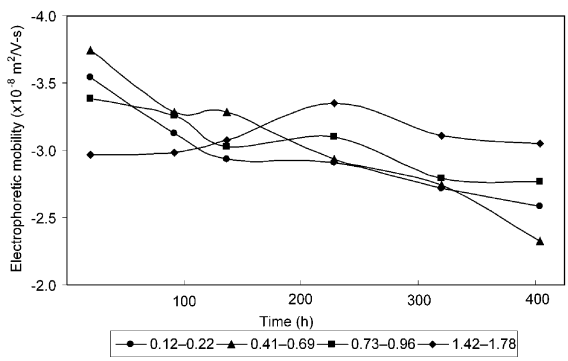

Figure 4. Change in electrophoretic mobility of nontronite particles with time during bioreduction for the same four size fractions of nontronite.

Particle aggregation as a result of bioreduction

Using the SEM method, nontronite particle aggregation kinetics were studied. In comparison with the treatment without shaking (Figure 1a), the aggregation rate appeared to be fast with shaking (Figure 5). Again, nontronite particles in the finer size fractions aggregated faster than those in the coarser size fractions. In 384 h, the D_{95} value increased by a factor of 43.7 and 7.7 for the 0.12−0.22 μm and the 1.42−1.78 μm fractions (Figure 6), respectively. Particle aggregation was also observed for the controls, with increase in the D_{95} value by a factor of 4.6 and 1.8 for the same two fractions, respectively (Figure 6). The SEM images of aggregated nontronite particles for the 0.12−0.22 μm fraction (384 h of bioreduction) (Figure 7a) showed that individual particles were bound together by polysaccharide. Despite the elongated and platy shape of individual particles in unreduced nontronite, the ultimate shape of aggregates tended to be spherical. The particle aggregation as a result of Fe(III) reduction for the 0.12−0.22 μm fraction was also confirmed by TEM (Figure 7b). Clay mixtures with biopolymers (see arrows) were attached to bacterial cells (CN 32) producing aggregates. The particles attached to cell surfaces were identified as nontronite by the lattice-fringe images of the outlined area (1.1 nm spacing of fringes).

Particle aggregation of chemically reduced nontronite

The results from the bioreduction experiments demonstrated that the extent of particle aggregation was correlated with the extent of Fe(III) bioreduction. For example, the finest size fraction with the greatest extent of bioreduction (Figure 2a) showed the greatest extent of particle aggregation (Figure 6). However, the concentration of EPS was similar for all the size

https://doi.org/10.1346/CCMN.2007.0550108 Published online by Cambridge University Press

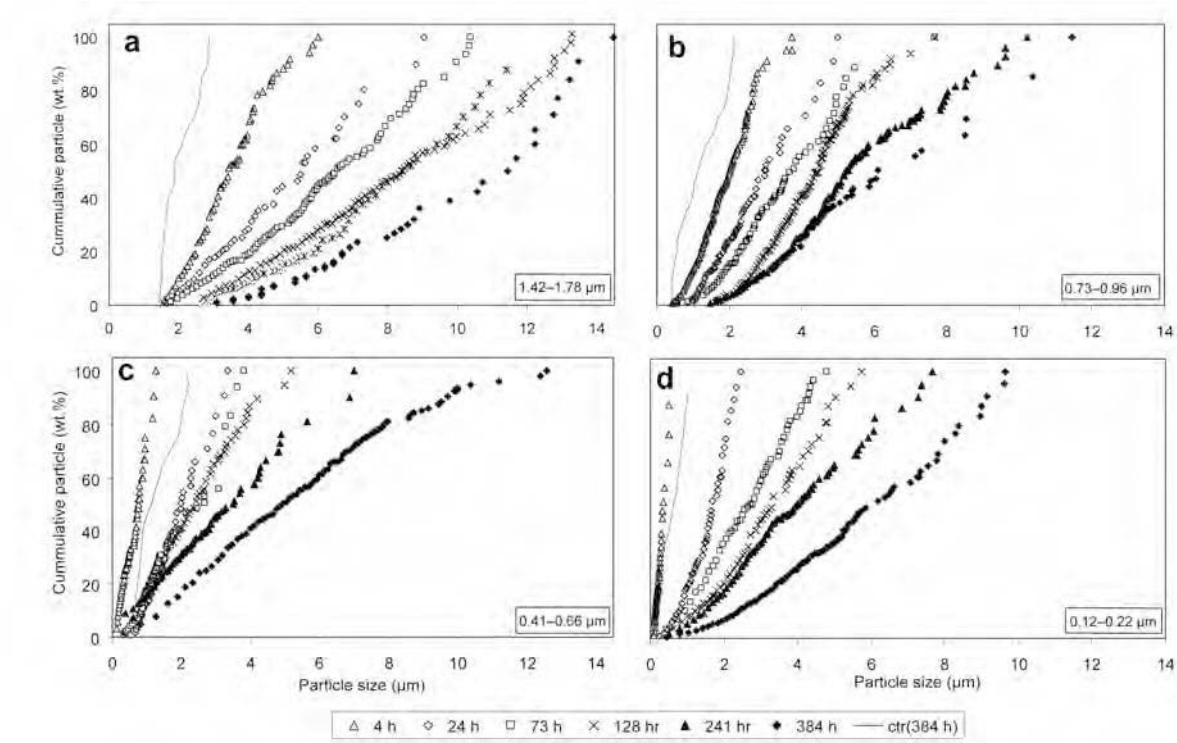

Figure 5. Time-course change in the particle-size distribution (as measured by SEM) over an extended period of Fe(III) bioreduction. The size fraction was 1.42−1.78 μm (a), 0.73−0.96μm (b), 0.41−0.69μm (c), 0.12−0.22 μm (d). The experiments were performed without Na pyrophosphate but with shaking. The ctr symbols denote abiotic control (384 h only).

fractions and showed no correlation with the extent of particle aggregation.

The results from chemically reduced nontronite confirmed that the rate of particle aggregation was indeed positively correlated with the extent of Fe(III) reduction. For example, for the size fraction of 0.73−0.96 μm, nontronite particles with its structural Fe(III) reduced to 17.5% showed a maximum increase in the D_{95} value by a factor of 6.1 within 132 h (Figure 8a). Nontronite particles with 38.0% reduction showed an increase in the D_{95} value by a factor 8.8 over the same duration (Figure 8b). When the extent of reduction was increased to 98%, nontronite particle size increased by a factor of 24.5 (data not shown). These data demonstrated the significant role of Fe(III) reduction in particle aggregation. The extent of aggregation for the controls was similar to that in the bioreduction experiments (limited to increase by a factor of 2.3 in 132 h).

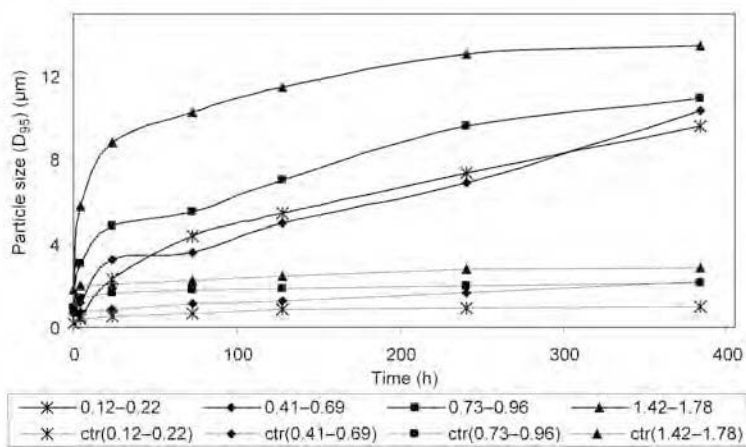

Figure 6. Time-course change in nontronite particle size at 95% percentile (D_{95}) (as measured by SEM) to illustrate more clearly the rate of nontronite particle aggregation during Fe(III) bioreduction. The data were taken from Fig. 5. The ctr symbols denote abiotic control.

https://doi.org/10.1346/CCMN.2007.0550108 Published online by Cambridge University Press

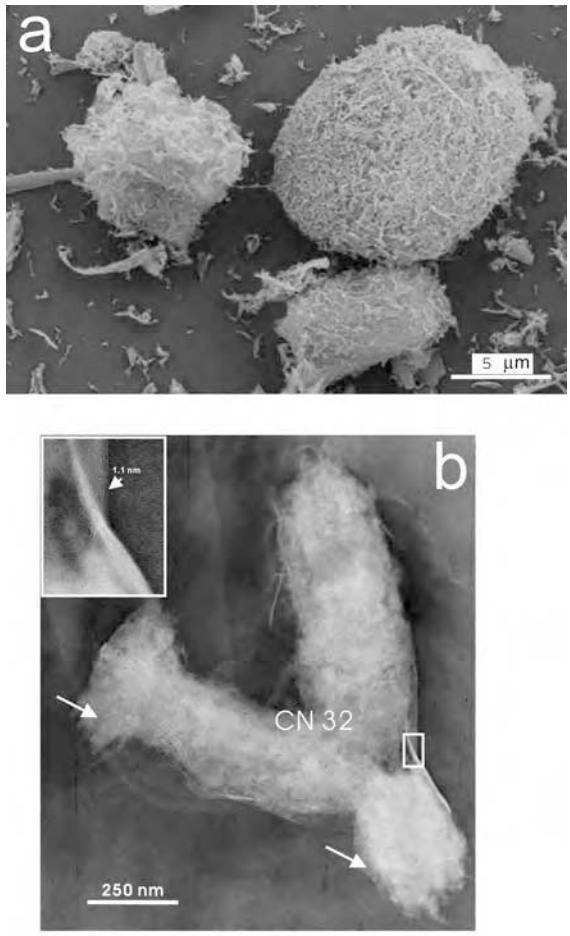

Figure 7. (a) SEM image showing aggregated particles of the 0.12–0.22 µm size fraction of nontronite after 384 h of bioreduction. The experiments were performed without Na pyrophosphate with shaking. Internal architecture was not apparent in these aggregates. (b) TEM image showing bioreduced clay particle mixtures with biopolymers (see the arrows) and bacteria (CN 32) promoting aggregation. The magnified outlined area shows clay structure fringes with 1.1 nm spacings.

In the chemically reduced nontronite, decreasing pH to the point of zero net proton charge (P_{ZNPC}) for NAu-2 (pH = 2.1) resulted in desorption of cations. There was a steady release of Si and Fe with an increased extent of Fe(III) reduction (Figure 9). The measured concentration of other cations (Ca, Mg, Al) remained nearly constant. An SEM image of aggregated particles in chemically reduced nontronite shows an array of clay plates and needles arranged in face-to-face and edge-to-face orientation (Figure 10).

Particle aggregation due to EPS bridging

When EPS extracted from CN32 cells was added to unreduced nontronite (0.73–0.96 µm size fraction), the rate of particle aggregation was increased relative to that in its absence, illustrating the effect of polymer bridging on particle aggregation. Within the first 132 h the D_{95} value increased by a factor of 4.1 and 6.5 for 50 mg/L and 800 mg/L EPS concentration, respectively (Figure 11).

A comparison was made for nontronite particle aggregation as a result of both Fe(III) reduction and polymer bridging, Fe(III) reduction only, and polymer bridging only. For the size fraction 0.73–0.96 µm, by the end of 132 h, the extent of Fe(III) bioreduction reached ~20% (Figure 2a) and the total EPS production was 50 mg/L. During this time frame, nontronite particle size increased by a factor of 7.3 as a result of both Fe(III) reduction and EPS bridging (Figure 6), compared with 6.1 from Fe(III) reduction only (Figure 8a) and 4.1 from polymer bridging only (Figure 11a). Such a comparison (Figure 12) revealed that both Fe(III) reduction and polymer bridging played an important role in clay particle aggregation.

The aggregates in the presence of EPS showed that individual clay particles were assembled together by EPS (Figure 13). Individual clay plates were attached in face-to-face orientations. The relative orientation of clay plates within an aggregate was random. This mode of aggregation was different from that in chemically reduced clay particles.

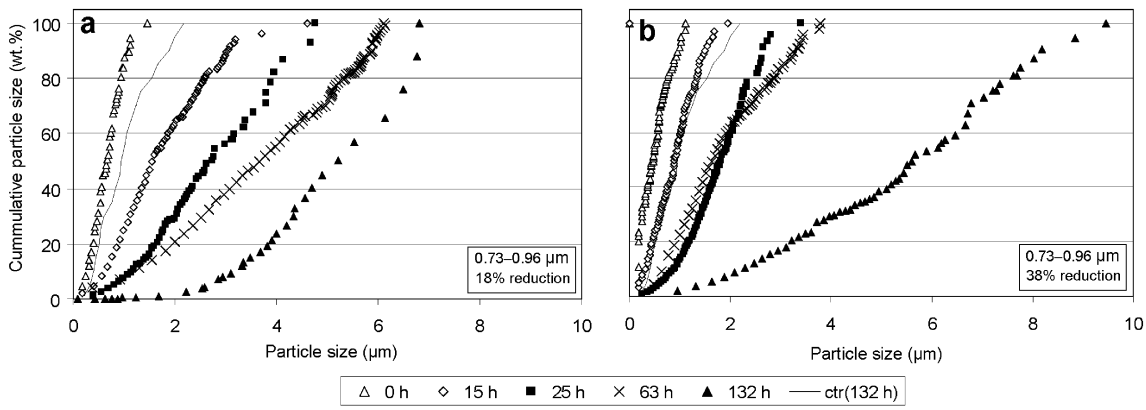

Figure 8. Change in particle-size distribution of nontronite particles that were pre-reduced to 18% (a) and 38% (b) by Na dithionite. The original size fraction was 0.73–0.96 µm. The ctr symbols denote abiotic controls (132 h only).

https://doi.org/10.1346/CCMN.2007.0550108 Published online by Cambridge University Press

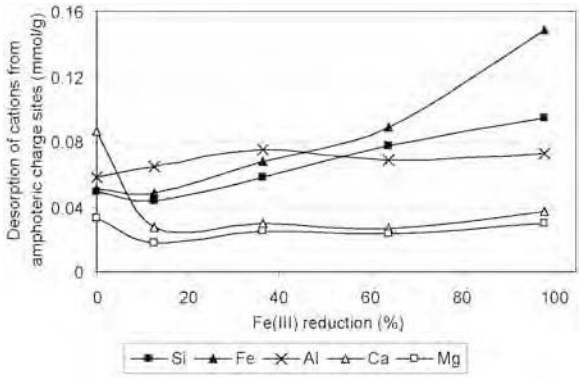

Figure 9. Release of surface-sorbed cations as a result of decrease in pH. The reduced nontronite was washed four times with anaerobic Na_2HCO_3 buffer, and dispersed again in the fresh buffer followed by lowering pH to the point of zero net charge for nontronite (2.1). The vertical axis is the difference in aqueous cation concentration at neutral pH (7.0) and pH 2.1.

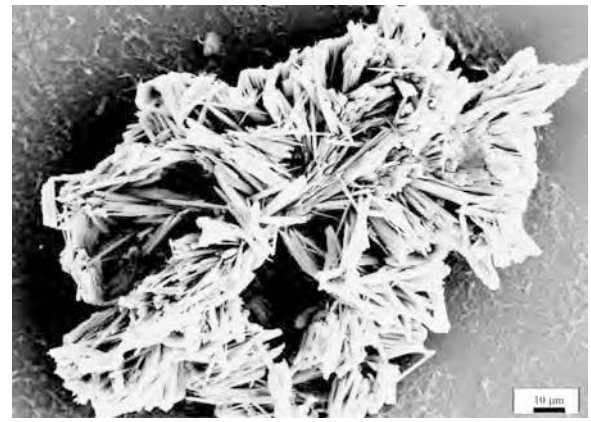

Figure 10. SEM image showing aggregated particles of chemically reduced nontronite. Most clay plates are aggregated in face-to-face and face-to-edge orientations.

DISCUSSION

Particle-size dependency of the extent of Fe(III) bioreduction

The greater rate and extent of Fe(III) reduction for the finer size fractions than for the coarser ones was probably due to the larger effective surface area of the small particle sizes. However, the surface area normalized extent of Fe(III) reduction was actually lower for the finer three size fractions than for the coarsest one (Figure 2b). One possible explanation may be related to the availability of Fe(III) surface sites. Because particle aggregation occurred much faster in the three fine fractions than in the coarsest one (Figures 5, 6), the measured surface area may not be entirely available for bioreduction, despite the fact that CN32 cells are capable of producing soluble electron shuttling compounds (Lovely *et al.*, 2004).

Particle aggregation as a result of bioreduction

Our collective results have revealed three important factors in controlling clay particle aggregation: (1) Fe(III) reduction; (2) change in bulk surface charge of nontronite; and (3) EPS production. The role of each of these factors will be discussed below.

Role of Fe(III) reduction in particle aggregation. There were three possible explanations for particle aggregation as a result of Fe(III) reduction: (1) increased van der Waals attraction; (2) cation bridging effect; and (3) charge heterogeneity. Firstly, despite the increase in bulk negative charge of individual nontronite particles and thus stronger electrostatic repulsion as a result of Fe(III) reduction, the attractive van der Waals force may still increase to result in particle aggregation. Secondly, some positively charged cations may be released to aqueous solution from reductive dissolution of nontronite (Dong *et al.*, 2003) (Figure 9) and subsequently

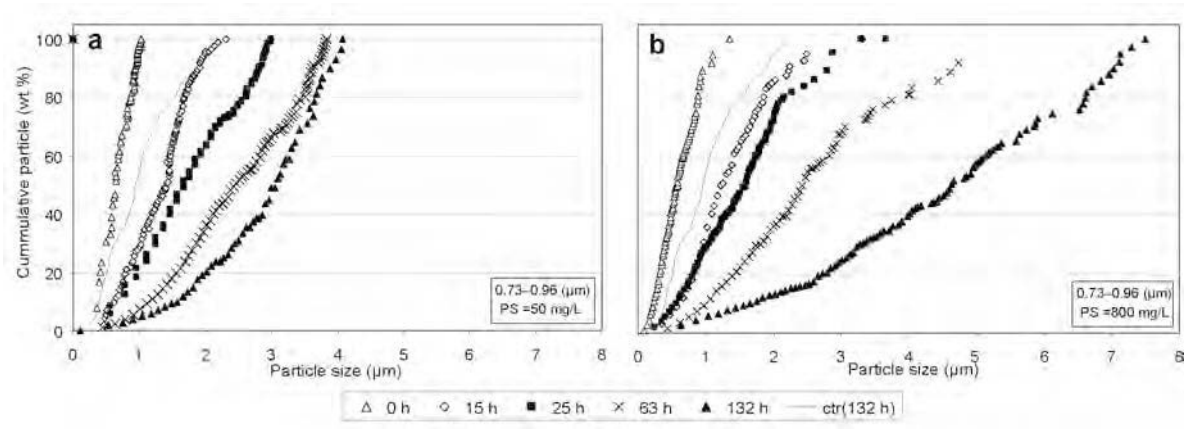

Figure 11. Particle aggregation due to addition of exopolysaccharide secreted by CN32 cells at a concentration of 50 mg/L (a) and 800 mg/L (b). The particle size at the start of the experiment was 0.73−0.96 µm. The ctr symbols denote abiotic controls (132 h).

https://doi.org/10.1346/CCMN.2007.0550108 Published online by Cambridge University Press

sorbed onto nontronite surfaces. An increase in electron density and proton attraction at the surface oxygen (Cervini-Silva *et al.*, 2000) induced by Fe(III) reduction may have enhanced sorption of cations. Sorbed cations could have bridged negatively charged nontronite particles and promoted particle aggregation. The cation bridging effect has been observed in the past and is expected to play an important role in promoting particle aggregation in natural processes (Boily and Fein, 1998). This effect may be similar to that of increased ionic strength in solution. For example, a high rate of aggregation of nano-clay particles was observed at a high ionic strength (Kotylar *et al.*, 1996). Flocculation of kaolinite was also enhanced by addition of Fe in aqueous solution (Arias *et al.*, 1995; Follett, 1965). Thirdly, as a result of Fe(III) reduction, nontronite particles may have developed localized charges, *i.e.* charge heterogeneity (Malla *et al.*, 1993), which would result in additional attraction. Charge heterogeneity may have been responsible for edge-to-face and cation bridging for face-to-face associations (Figure 10).

Role of bulk surface charge of nontronite in particle aggregation. As clay aggregates grew with time, the bulk surface charge of aggregates may play a more dominant role than the layer charge of individual nontronite particles (Theng, 1979). In a system where there is a mixture of coarse aggregates and fine individual particles, the overall surface charge may be dominated by the large aggregates. When a fine particle approaches a large aggregate (formed from previous aggregation), the negative charge of the small particle may be reversed or decreased due to the induction effect from the larger aggregates (Overbeek, 1988). So the overall surface charge of an aggregate, as measured by electrophoretic mobility, may be less negative than the sum of all constituent particles. This charge reversal effect would promote coarsening of a limited number of previously formed aggregates, as observed in our experimental data (Figures 1, 5 and 6). The formation of large aggregates would in turn trigger more charge reversals of small particles, which would result in further aggregation. This positive feedback mechanism was actually observed in our experimental data, where the significant extent of particle aggregation (0.12–0.22 μm fraction) corresponded to high charge reversal (the EPM values becoming less negative with time in Figure 4).

Role of polysaccharide in particle aggregation. *Shewanella putrefaciens* CN32 cells can produce polysaccharide that is composed of core oligosaccharide and lipid A backbone without capsular surface polysaccharide (Korenevsky *et al.*, 2002; Nazarenko *et al.*, 2004). The highly ionizable surface groups on the oligosaccharide backbone (such as phosphate and carboxylate groups) (Korenevsky *et al.*, 2002) may provide sites for clay particle attachment, if they are exposed. Such an attachment may explain the associations between nontronite particles and polysaccharide/bacteria (Figures 7, 13). This attachment process may be similar to that used by *E. coli* cells to attach to particle surfaces through chemical interaction of its EPS (Walker *et al.*, 2004). Since CN32 cells also release free and surface-attached EPS and other electron shuttling compounds into the solution (Lovley *et al.*, 2004) to enhance Fe(III) reduction, particle bridging by these compounds may also be a viable mechanism for clay particle aggregation.

When the polysaccharide excreted by CN32 cells was isolated and added to unreduced nontronite, the rate of particle aggregation was enhanced (Figure 11a,b) relative to the control without EPS addition. This result strongly suggests that CN32 polysaccharide played an important role in clay particle aggregation. However, the mechanism of particle attachment by isolated polysaccharide may be different from that of living cells, and thus its role in clay aggregation was expected to be

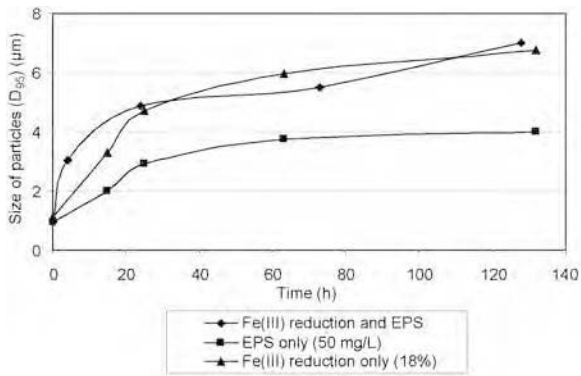

Figure 12. Time-course change in particle size (at D_{95}) showing a comparison among three systems: both Fe(III) reduction and exopolysaccharide, Fe(III) reduction only, and exopolysaccharide only. The particle size at the start of the experiment was 0.73–0.96 μm in each case.

Figure 13. SEM image showing aggregation of native nontronites as a result of addition of pure exopolysaccharide extracted from CN32 cells. In contrast to the texture of aggregation as a result of Fe(III) reduction (Figure 10), this exopolysaccharide-promoted aggregation shows a random orientation of nontronite particles with respect to one another.

https://doi.org/10.1346/CCMN.2007.0550108 Published online by Cambridge University Press

different. For example, whereas the cell-associated polysaccharide appeared to be interacting with individual nontronite particles (Figure 7a), the isolated polysaccharide appeared to be wrapping around multiple clay particles to form a large aggregate (Figure 13).

Our method of separating the effect of Fe(III) bioreduction and EPS production represented one step forward. Although it was our initial intention to quantify the relative role of Fe(III) bioreduction and polysaccharide production in clay particle aggregation, it was premature to do so at present for the reasons described above. Nonetheless, our data definitely demonstrated that both Fe(III) reduction and polysaccharide played a significant role in clay aggregation.

Implications for clay particle aggregation in natural environments

Our experiments were performed under anoxic conditions, where CN32 cells reduced Fe(III) in nontronite and produced polysaccharide, both of which contributed to nontronite particle aggregation. However, in natural environments, Fe(III) bioreduction and polysaccharide production may not take place at the same time. When conditions become oxic, Fe(III) reduction activity ceases, but polysaccharide may still be produced. In such cases, polysaccharide may play a dominant role. Therefore, it is important to consider environmental conditions when the relative importance of these two factors, *i.e.* Fe(III) reduction and polysaccharide production, is evaluated.

CONCLUSIONS

In this study, we examined the effects of Fe(III) reduction and polysaccharide production on clay particle aggregation. When these two effects were considered together and separately, it was clear that nontronite particle aggregation was controlled by both the redox state of Fe in the nontronite structure and production of polysaccharide by bacterial cells during Fe(III) reduction. Our quantitative data showed that Fe(III) reduction probably played a more important role. However, the relative importance of these two effects may be dependent on the nature of a particular system (such as redox conditions and rate and extent of polysaccharide supply).

ACKNOWLEDGMENTS

This research was supported by a grant from National Science Foundation (EAR-0345307). Some of this research was supported by student grants from The Clay Minerals Society (Student Research Grant, 2004) and AAPG (John Teagle Memorial Grant, 2004) to DPJ. We are grateful to two anonymous reviewers and Associate Editor Crawford Elliott for their constructive criticisms which helped to improve the quality of the manuscript. JWK publishes with NRL contribution number NRL/JA/7430-06-05.

REFERENCES

Arias, M., Barral, T. and Diaz-Fierros, F. (1995) Effects of iron and aluminum oxides on the colloidal and surface properties of kaolin. *Clays and Clay Minerals*, **43**, 406–416.

Boily, J. and Fein, J.B. (1998) Adsorption of Pb(II) and benzenecarboxylates onto corundum. *Chemical Geology*, **148**, 157–175.

Bradford, M.M. (1976) A rapid and sensitive method for the quantization of microgram quantities of protein utilizing the principle of protein-dye binding. *Analytical Biochemistry*, **1/2**, 248–254.

Bura, R., Chung, M., Liao, B., Finlayson, J., Lee, B.C., Droppo. I.G., Lepard, G.G. and Liss, S.N. (1998) Composition of extracellular polymeric substances in the activated sludge matrix. *Water Science and Technology*, **37**, 325–333.

Cervini-Silva, J., Wu, J., Stucki, J.W. and Larson, R.A. (2000) Adsorption kinetics of pentachloroethane in iron-bearing smectites. *Clays and Clay Minerals*, **48**, 132–138.

Chenu, C., Pons, C.H. and Robert, M. (1979) Interaction of kaolinite and montmorillonite with neutral polysaccharide. *Proceedings of International Clay Conference*, Denver, Colorado, The Clay Minerals Society.

Dachs, J. and Bayona, J.M. (1997) Langmuir-derived model for diffusion- and reaction-limited adsorption of organic compounds on fractal aggregates. *Environmental Science and Technology*, **31,** 2754–2760.

de Boodt, M.F. (1990) *Application of Polymeric Substances as Physical Soil Conditioners. Soil Colloids and their Association in Aggregates* (M.F. de Boodt, M.H. Hays, A. Herbillon, editors). Plenum Press, New York pp. 517–556.

Dong, H. (2002) Significance of electrophoretic mobility distribution to bacterial transport. *Journal of Microbiological Methods*, **51**, 83–93.

Dong, H., Kostka, J.E. and Kim, J.W. (2003) Microscopic evidence for microbial dissolution of smectite. *Clays and Clay Minerals*, **51**, 502–512.

Droppo, I.G. and Irvine, K.N. (2002) Flocculation/aggregation of cohesive sediments in the urban continuum: Implications for storm water management. *Environmental Technology*, **23**, 27–41.

Dubois, M., Gilles, K.A., Hamilton, J.K., Rebers, P.A. and Smith, F. (1956) Colorimetric method for determination of sugars and related substances. *Analytical Chemistry*, **28,** 350–356.

Elimelech, M., Gregory, J., Jia, X. and Williams, R.A. (1995) *Particle Deposition and Agglomeration: Measurement, Modeling and Simulation.* Butterworth-Heinemann Ltd., London.

Follett, E.C. (1965) The retention of amorphous, colloidal ferric hydroxide by kaolinite. *Journal of Soil Science*, **16**, 334–341.

Fredrickson, J.K., Zachara, J.M., Kennedy, D.W., Dong, H., Onstott. T.C., Hinman, N.W. and Li, S. (1998) Biogenic iron mineralization accompanying the dissimilatory reduction of hydrous ferric oxide by a groundwater bacterium. *Geochimica et Cosmochimica Acta*, **62**, 3239–3257.

Fuller, L., Goh, T.B., Oscarson, D.W. and Biliaderis, C.G. (1995) Flocculation and coagulation of Ca- and Mg-saturated montmorillonite in the presence of a neutral polysaccharide. *Clays and Clay Minerals*, **43**, 533–539.

Gates, W.P., Wilkinson, H.T. and Stucki, J.W. (1993) Swelling properties of microbially reduced ferruginous smectite. *Clays and Clay Minerals*, **41**, 360–364.

Gates, W.P., Jaunet, A., Tessier, D., Cole, M.A., Wilkinson, H.T. and Stucki, J.W. (1998) Swelling and texture of iron bearing smectites reduced by bacteria. *Clays and Clay Minerals*, **46**, 487–497.

https://doi.org/10.1346/CCMN.2007.0550108 Published online by Cambridge University Press

Healy, T.W. and La Mer, V.K (1964) Energetics of flocculation and redispersion by polymers. *Journal of Colloid and Interface Science*, **19**, 323–332.

Hill, P.S. (1996) Sectional and discrete representations of floc breakage in agitated suspensions. *Deep Sea Research I*, **43**, 679–702.

Hill, P.S., Voulgaris, G. and Trowbridge, J.H. (2001) Controls on floc size in a continental shelf bottom boundary layer. *Journal of Geophysical Research – Oceans*, **106**, 9543–9549.

Hoggs, R. (1984) Collision efficiency factors for polymer flocculation. *Journal of Colloid and Interface Science*, **102,** 232–236.

Hunter, R.J. (1981) *Zeta Potential in Colloidal Science: Principles and Applications*. Academic Press, New York.

Jaisi, D.P., Kukkadapu, R.K., Eberl, D.D. and Dong, H. (2005) Control of Fe(III) site occupancy on the rate and extent of microbial reduction of Fe(III) in nontronite. *Geochimica et Cosmochimica Acta*, **69,** 5429–5440.

Katoh, S., Danhara, T., Hart, W.K. and Wolde-Gabriel, G. (1999) Use of sodium polytungstate solution in the purification of volcanic glass shards for bulk chemical analysis. *Natural Human Acta*, **4**, 45–54.

Keeling, J.L., Raven, M.D. and Gates, W.P. (2000) Geology and characterization of two hydrothermal nontronites from weathered metamorphic rocks at the Uley graphite mine, South Australia. *Clays and Clay Minerals,* **48,** 537–548.

Kim, J.W., Dong, H., Seabaugh, J., Newell, S.W. and Eberl, D.D. (2004) Role of microbes in the smectite-to-illite reaction. *Science*, **303**, 830–832.

Kim, J.W., Furukawa, W., Dong, H. and Newell, S.W. (2005) The role of microbial Fe(III) reduction in clay flocculation. *Clays and Clay Minerals,* **53**, 572–579.

Korenevsky, A.A., Vinogradov, E., Gorby, Y. and Beveridge, T.J. (2002) Characterization of the lipopolysaccharides and capsules of *Shewanella spp*. *Applied and Environmental Microbiology*, **68,** 4653–4657.

Kostka, J.E., Stucki, J.W., Nealson, K.H. and Wu, J. (1996) Reduction of structural Fe(III) in smectite by a pure culture of *Shewanella putrefaciens* strain MR-1. *Clays and Clay Minerals*, **44**, 522–529.

Kostka, J.E., Haefele, E., Viehweger, R. and Stucki, J.W. (1999a) Respiration and dissolution of iron(III)-containing clay minerals by bacteria. *Environmental Science and Technology*, **33**, 3127–3133.

Kostka, J.E., Wu, J., Nealson, K.H. and Stucki, J.W. (1999b) The impact of structural Fe(III) reduction by bacteria on the surface chemistry of smectite clay minerals. *Geochimica et Cosmochimica Acta*, **63,** 3705–3713.

Kotylar, L.S., Sparks, B.D. and Schutte, R. (1996) Effect of salt on the flocculation behaviors of nano particles in oil sands fine tailings. *Clays and Clay Minerals*, **44,** 121–131.

Liao, B.Q., Allen, D.G., Droppo, I.G., Leppard, G.G. and Liss, S.N. (2001) Surface properties of sludge and their role in bioflocculation and settleability. *Water Research*, **35**, 339–350.

Lovley, D.R., Holmes, D.E. and Nevin, K.P. (2004) Dissimilatory Fe(III) and Mn(IV) reduction. *Advances in Microbial Physiology*, **49**, 219–286.

Malla, P.B., Robert, M., Douglass, L.A., Tessier, D. and Komarneni, S. (1993) Charge heterogeneity and nanostructure of 2:1 layer silicates by high resolution transmission electron microscopy. *Clays and Clay Minerals*, **41**, 412–422.

Moore, D.M. and Reynolds, R.C., III (1997) *X-ray Diffraction and the Identification and Analysis of Clay Minerals*. Oxford University Press, New York.

Moudgil, B.M., Shah, B.D. and Suto, H.S. (1987) Collision efficiency factors in polymer flocculation of fine particles. *Journal of Colloid and Interface Science,* **119,** 466–473.

Nazarenko, E.L., Nadezhda A., Komandrova, N.A., Gorshkova, R.P., Tomshich, S.V., Zubkov, V.A., Kilcoyne, M. and Savage, A.V. (2004) Structures of polysaccharides and oligosaccharides of some gram negative marine proteobacteria. *Carbohydrate Research*, **338**, 2449–2457.

Olness, A. and Clapp, C.E. (1975) Influence of polysaccharide structure on the dextran adsorption by montmorillonite. *Soil Biology and Biochemistry*, **7,** 113–118.

O'Melia, C.R. (1980) Aquasols: the behavior of small particles in aquatic systems. *Environmental Science and Technology*, **14**, 1052–1060.

Orton, P.M. and Kineke, G.C. (2001) Comparing calculated and observed vertical suspended-sediment distributions from a Hudson River Estuary turbidity maximum. *Estuarine Coastal and Shelf Science*, **52**, 401–410.

Overbeek, J.T.G. (1988) Double layer interaction between spheres with unequal surface potentials. *Journal of the Chemical Society Faraday Transactions I*, **84,** 3079–3091.

Pignatello, J.J. and Xing, B. (1996) Mechanisms of slow sorption of organic chemicals to natural particles. *Environmental Science and Technology*, **30**, 1–5.

Stookey, L.L. (1970) Ferrozine – a new spectrophotometric reagent for iron. *Analytical Chemistry***, 42**, 779–781.

Stucki, J.W. (2006) Iron redox processes in clay minerals. Chapter 8 in: *Handbook of Clay Science* (F. Bergaya, G. Lagaly and B.K.G. Theng, editors). Elsevier, Amsterdam.

Stucki, J.W., Lee, K., Zhang, L. and Larson, R.A. (2002) The effects of iron oxidation state on the surface and structural properties of smectites. *Pure and Applied Chemistry*, **74**, 2079–2092.

Stucki, J.W., Low, F.P., Roth, C.B. and Golden, D.C. (1984) Effects of oxidation state of octahedral iron on clay swelling. *Clays and Clay Minerals*, **32**, 357–362.

Tallon, R., Bressollier, P. and Urdaci, M.C. (2003) Isolation and characterization of two exoploysachharides produced by *Lactobacillus plantarum* EP 56. *Research in Microbiology*, **154**, 705–712.

Theng, B.K.G. (1979) *Formation and Properties of Clay-Polymer Complexes.* Elsevier Scientific Publishing Co., Amsterdam.

Theilen, F.R. and Pecher, I.A. (1991) Assessment of shear strength of the sea bottom from shear wave velocity measurements on box cores and in situ. Pp. 67–74 in: *Shear Wave in Marine Sediments* (J.M. Hoven *et al*., editors). Kluwer Academic Publishers, Dordrecht, The Netherlands.

Tolhurst, T.J., Gust, G. and Paterson, D.M. (2002) The influence of an extra cellular polymeric substance (EPS) on cohesive sediment stability Pp. 409–425 in: *Fine Sediment Dynamics in the Marine Environment* (J.C. Winterwerp and C. Kranenburg, editors). Proceedings in Marine Science, **5**. Elsevier Science, Amsterdam.

Walker, H.W. and Bob, M.M (2001) Stability of particle flocs upon addition of natural organic matter under quiescent conditions. *Water Research***, 35,** 875–882.

Walker, S.L., Redman, J.A. and Elimelech, M. (2004) Role of cells surface lipopolysaccharides in *Escherichia coli* K12 adhesion and transport. *Langmuir,* **20,** 7736–7746.

Xu, R. (1993) Methods to resolve mobility from electrophoretic laser light scattering measurement. *Langmuir*, **9,** 2955–2962.

Yuehena, H., Wei, S., Haipu, L. and Xu, Z. (2004) Role of macromolecules on kaolinite floatation. *Minerals Engineering*, **17**, 1017–1022.

(*Received 9 May 2006; revised 2 September 2006; Ms. 1175; A.E. W. Crawford Elliot*)

https://doi.org/10.1346/CCMN.2007.0550108 Published online by Cambridge University Press